JOURNAL OF GUIDANCE, CONTROL, AND DYNAMICS
Vol. 29, No. 5, September–October 2006

Unmanned Aerial Vehicle Path Following for Target Observation in Wind

Rolf Rysdyk*
University of Washington, Seattle, Washington 98195

This work provides flight-path geometry, guidance laws, and synchronous camera angles to observe a ground target from an unmanned aerial vehicle. The observation of the target is affected by wind, aircraft performance, and camera limits. Analytic expressions are derived for paths that result in constant line-of-sight orientation of the target relative to the aircraft body frame. Using minimal heuristics, a guidance law based on "good helmsman" behavior is developed and implemented, and stability of its integration with aircraft dynamics is assessed. An observer estimates wind data, which are used to orient path geometry about the target. Results are demonstrated in high-fidelity simulation.

Nomenclature

a	=	helmsman sensitivity parameter
$c_{(\cdot)}$	=	$\cos(\cdot)$
d	=	distance
$\mathcal{F}_b$	=	body-fixed frame
$\mathcal{F}_s$	=	Serret–Frenet frame
g	=	gravity constant
r	=	radius
s	=	arclength position along desired path
$s_{(\cdot)}$	=	$\sin(\cdot)$
$t_{(\cdot)}$	=	$\tan(\cdot)$
$\boldsymbol{V}$	=	velocity
V_a	=	airspeed
V_g	=	inertial speed (ground speed)
V_w	=	windspeed (inertial)
$\boldsymbol{x}_b, \boldsymbol{y}_b, \boldsymbol{z}_b$	=	body-fixed axes system
$\boldsymbol{x}_N, \boldsymbol{y}_E, \boldsymbol{z}_D$	=	navigation axes system
x, y, z	=	position coordinates
$\hat{\boldsymbol{x}}$	=	observer state vector
y_s	=	cross-track error
α	=	angle of attack
β	=	angle of sideslip
ζ	=	bearing angle of target from the aircraft
κ	=	camera pan angle
$\kappa(s)$	=	curvature of desired path at position s
λ	=	camera tilt angle
ρ	=	radius of curvature
ϕ	=	bank angle
χ	=	course
χ_s	=	desired course on orbit
χ_w	=	wind direction ("from" convention)
ψ	=	heading
ψ_p	=	bearing angle of aircraft from the target ("clock angle" relative to target)
ψ_w	=	wind vector orientation ($\psi_w = \chi_w + \pi$)

Subscripts and Supersripts

ac	=	aircraft center of gravity
b	=	body-fixed reference frame
c	=	command
e	=	Earth reference frame
icpt	=	Intercept
m	=	measured
s	=	Serret–Frenet reference frame
tgt	=	target
w	=	wind
$\wedge$	=	estimate

Received 25 July 2005; revision received 17 November 2005; accepted for publication 21 November 2005.

*Assistant Professor, Department of Aeronautics and Astronautics; rysdyk@aa.washington.edu. Member AIAA.

I. Introduction

THE objective of this work is to provide algorithms for flight-path guidance and synchronous camera angles to observe a target from an unmanned aerial vehicle (UAV).[1] Semiautonomous operation of UAVs for target sensing have shown that operator situational awareness can easily be compromised when the target goes out of sight. The observation may be affected by sunlight angles, maximum aircraft performance, and camera limits.[2] In this work trajectories are proposed and a guidance law is designed that results in *constant-line-of-sight orientation* relative to the aircraft. An example of constant-line-of-sight path geometry is one that aims the UAV wingtip at the target throughout the maneuver, colloquially referred to as "turn-on-a-pylon." This maneuver effectively decouples the problem of aiming the camera from that of aircraft guidance and control.

Typically, when a target is observed from a small UAV, camera aim is coupled to the characteristics of the aircraft. This coupling is due to sensor limitations and UAV kinematic characteristics, for example, Refs. 1–5. In Ref. 5 the authors extend the recursive path-following algorithm of Ref. 6 to the coordinated control of aircraft and camera with the aim of keeping a specified landmark in sight. A further interesting challenge is the tracking of a moving target, which is an ongoing effort.[3,4,7]

Providing accurate path following (or trajectory tracking, which includes timing) is a key challenge in obtaining full autonomy for UAVs.[8] For accurate path-following, the guidance and control system feedback loops may have overlapping bandwidth. Therefore, a stability assessment should include the coupling of guidance and control elements. References 9–11 provide a nonlinear analysis of coupled guidance and control loops and provide explicit stability conditions for the time constant of the control loop relative to that of the guidance loop. Reference 12 provides background material, as well as a stability analysis for integrated guidance and control design. Guidance systems are enhanced by explicitly including maneuvering capabilities and switching between position convergence and timing priority as presented in Refs. 13 and 14. Similar approaches with consideration of convergence properties are discussed in Refs. 15 and 16, which are amenable to feedback linearization and backstepping methods. Path-following convergence is also affected by the shape, or aggressiveness, of the desired path. In many of

the applications to autonomous vehicles, some a priori information on the path is assumed available, and often the assumption is made that paths can be constructed of line segments with a constant curvature. This is the case in variations of proportional navigation methods, recent, examples of which include Refs. 11, 17, and 18. (The "constant-line-of-sight orientation" in the objective of the current work is not to be confused with the "line-of-sight guidance" of proportional navigation methods.) In Ref. 11 constant curvature is approached with an explicit feedforward element, which is also done in the current work. The guidance logic in Ref. 18 implicitly contains anticipatory action for convergence with curved paths. Reference 19 presents an approximate path-following algorithm based on a notion of convergence to within a "tube" around the desired path, significantly reducing reliance on a priori path information.

Guidance systems for autonomous UAVs typically involve the following degrees of freedom: airspeed, aerodynamic sideslip angle, turn rate, and flight-path angle. With most conventional aircraft, these are controlled with aerodynamic surfaces (ailerons, elevator, and rudder) about three body axes and the propulsion source (throttle). The aircraft under consideration includes control laws for altitude-hold and airspeed-hold using throttle and elevator and automatic turn coordination using rudder. This leaves the ailerons to address the course deviation problem. The ailerons control the aircraft roll degree of freedom and hence the bank angle.

The bank angle in a steady state coordinated turn is kinematically related to the heading rate of turn. For design of the guidance feedback loop, the aircraft bank angle may be considered as the control variable. The guidance problem consists of stabilizing two degrees of freedom to zero: course angle error and cross-track error. One approach to such guidance problems is to couple the commanded course to the measured cross-track error.[20] In this work we accomplish this by modeling the path following behavior of a "good helmsman."[21]

Because of the nature of the observation orbits, we rely on convergence to prespecified paths. The observation orbits require only slowly varying trajectories and therefore it is possible to take the aircraft capabilities into account in their design. However, a more general approach is used here that provides robustness with respect to wind and aircraft limitations. The stability of the combined guidance and control scheme is assessed.

A Serret–Frenet formulation is used to represent the vehicle kinematics in terms of path parameters, which allows for convenient definition of cross-track and course error. The integration of a Serret–Frenet based guidance law and a turn-coordination control inner loop will compensate for wind. Results are demonstrated for a small UAV[22] by simulation of nonlinear flight and sensor dynamics operating in an environmental model.[23]

II. Guidance and Control Law Development

In design of the guidance law, the aim is smooth convergence with the desired path using minimal heuristics. The path-following structure will obtain a command from a path-planner algorithm,[24] which provides desired waypoints with splining of straight lines and curves. A secondary aim is to relieve the path planner of the computational burden of producing "feasible" paths. Feasibility in this case pertains to aircraft performance constraints, possibly dependent on operating conditions. The Serret–Frenet formulation allows convenient parameterization of the desired path in terms of aircraft natural motion, this provides analytical advantages[12] and convenient guidance command design.

A. Serret–Frenet Formulation for Path Following in the Horizontal Plane

The objective of this section is to express the vector of vehicle velocity relative to the desired (two-dimensional) path in the horizontal plane. The relative position is measured from the vehicle to the "closest" point on the desired path, as implied by a perpendicular projection, Fig. 1. If we consider a frame $\mathcal{F}_s$ along the desired path, with its x-axis in the direction of the desired inertial velocity, that is, tangential to the path, and its y-axis normal to the path. Let s be the arclength along the desired path. With s indicating a position on the

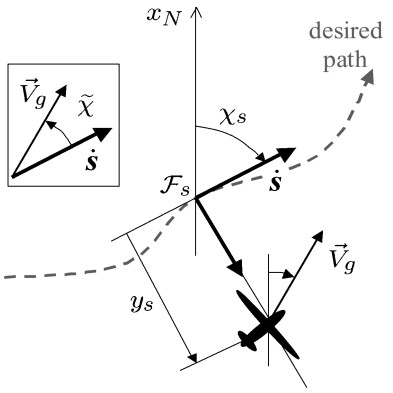

Fig. 1 The "Serret–Frenet" frame for a path in the horizontal plane.

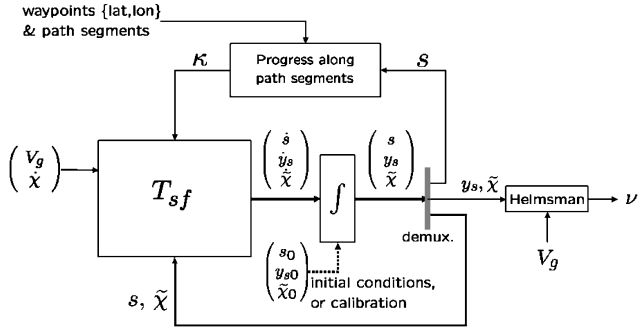

Fig. 2 The coordinate transformation integrated with the autonomous helmsman logic. Commanded path segments are received from a path planner/trajectory generator. The helmsman and its signals are described in Sec. II.B.

path, the curvature $\kappa(s)$ at that position is defined as $\kappa(s) = 1/\rho(s)$, where $\rho(s)$ is the radius of the path at that point. If the direction of the path is indicated as χ_s (which is considered the desired "course" when on the path) then the path parameters are related to yaw rate as

$$\dot{\chi}_s(s) = \kappa(s)\dot{s}$$

and the Serret-Frenet formulas in two-dimensional truly banked flight, result in the following transformation

$$\begin{pmatrix} \dot{s} \\ \dot{y}_s \\ \dot{\tilde{\chi}} \end{pmatrix} = T_{sf}(\tilde{\chi}, y_s, \kappa) \begin{pmatrix} V_g \\ \dot{\chi} \end{pmatrix} \tag{1}$$

where

$$T_{sf} \triangleq \begin{pmatrix} \dfrac{c_{\tilde{\chi}}}{(1-\kappa y_s)} & 0 \\ s_{\tilde{\chi}} & 0 \\ -\dfrac{c_{\tilde{\chi}}\kappa}{(1-\kappa y_s)} & 1 \end{pmatrix} \tag{2}$$

where χ is the flown course, and the *relative course* is defined as

$$\tilde{\chi} \triangleq \chi - \chi_s \tag{3}$$

Transformation (2) is not usable when $y_s = 1/\kappa(s) = \rho(s)$, that is, when the vehicle is at the center of the instantaneous circle. Equation (1) expresses the aircraft translational motion relative to the desired path. Its integration with the autonomous helmsman behavior is represented in Fig. 2.

B. Guidance Law Design: Helmsman Behavior

These expressions allow formulation of a guidance law that takes inertial velocity and cross-track error as input and provides a commanded heading rate as output.

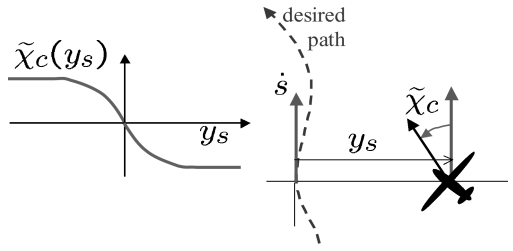

Fig. 3 The behavior of a "good helmsman" modelled by the desired relative course $\tilde{\chi}_c$ as a function of cross-track error y_s in the form of a sigmoid function (left), saturating at $\pm\tilde{\chi}_{\text{icpt}} \cdot \tilde{\chi}_c \approx 0$ when "close" to the trajectory, and saturates at $\tilde{\chi}_c = \pm\tilde{\chi}_{\text{icpt}}$ when farther away.

The guidance law objective is to converge $\tilde{\chi}$ and y_s simultaneously to zero. This may be achieved by coupling the commanded angle of convergence and cross-distance, that is, $\tilde{\chi}_c(y_s)$, Fig. 3. According to Ref. 21, the behavior of a "good helmsman" follows an intercept course $\tilde{\chi}_c$ that varies with cross track error y_s, rather than using sideward velocity. This is similar to an aircraft in coordinated flight, with the bank angle considered as the control variable.

The helmsman behavior relative to a straight-line course $\chi_s \equiv 0$ is

$$\chi_c = \sigma(y_s) \tag{4}$$

where χ_c represent the commanded absolute course, and $\sigma(y_s)$ is any function satisfying

$$y_s\sigma(y_s) < 0, \qquad y_s \neq 0$$
$$\sigma(0) = 0, \qquad \sigma : y_s \to [-\tilde{\chi}_{\text{icpt}}, \tilde{\chi}_{\text{icpt}}] \tag{5}$$

where $\tilde{\chi}_{\text{icpt}}$ represents the intercept angle at large cross-track error.

For interception and tracking of a curved path, the helmsman behavior is relative to that path. The helmsman behavior is then expressed by formulating the commanded course χ_c in terms of χ_s and y_s. In that case expression (4) becomes

$$\tilde{\chi}_c \triangleq \chi_c - \chi_s = \sigma(y_s) \tag{6}$$

Therefore, the helmsman behavior in trajectory tracking is

$$\chi_c(y_s, \chi_s) = \sigma(y_s) + \chi_s \tag{7}$$

Two aspects of the helmsman determine its "aggressiveness": the maximum intercept angle, and the "lead distance" or slope $\mathrm{d}\sigma/\mathrm{d}y_s$. For good path-following performance it is essential to focus on these convergence properties. Heuristic course trackers exist that obtain both efficiency and high precision, while taking advantage of maximum vehicle performance. In these trackers, to ensure smooth and fast convergence, the signal $(\mathrm{d}/\mathrm{d}t)\tilde{\chi}_c(y_s, V_g, \tilde{\chi})$ can be determined iteratively, based on relative location, orientation, and known aircraft bank performance. This is valuable, for example, in the UAV retrieval or autoland phase. The helmsman functions suggested in this paper may not obtain the same convergence performance without specific gain scheduling. However, they are well suited for more general trajectories, use a minimum of heuristics, and are robust with respect to wind and turbulence.

C. Control Signal Construction

In the following, a bank-angle command is constructed based on the helmsman behavior with the goal of following the desired path. It is assumed that the wind $\{V_w, \chi_w\}$ is known (or estimated; see, e.g., Sec. VI), the airspeed V_a and altitude remain approximately constant, bank-angle command following performs well and fast relative to path changes of ± 30 deg, and the commanded path will be mild enough to prevent extreme wind-up of path-following integral action due to roll-rate and saturation limits. The latter is a temporary assumption; hedging of the commanded heading rate can be implemented later.[25]

Let the ideal course convergence dynamics be specified as follows:

$$\frac{\mathrm{d}}{\mathrm{d}t}\chi(t) = \nu(\chi, \chi_c) \tag{8}$$

where "pseudocontrol" $\nu(\chi, \chi_c)$ refers to the "tracking-servo" control law. Defined in terms relative to the desired path, this may be written as

$$\frac{\mathrm{d}}{\mathrm{d}t}\{\chi - \chi_s\} = \nu(\chi - \chi_s, \chi_c - \chi_s) \Leftrightarrow \frac{\mathrm{d}}{\mathrm{d}t}\tilde{\chi} = \nu(\tilde{\chi}, \tilde{\chi}_c) \tag{9}$$

where χ_s is the direction of the desired path and χ_c is the commanded course. The guidance law may then be based on desired tracking dynamics by design of the pseudocontrol ν. Standard linear behavior can then be imposed.

To avoid adding integrator dynamics and its associated implementation woes, we used a simple proportional design with a feedforward term:

$$\nu = k_p(\tilde{\chi}_c - \tilde{\chi}) + \nu_\kappa \tag{10}$$

where $\nu_\kappa = \kappa V_g$ is a kinematics feedforward term that replaces the need for integral action for constant curvature path following (see the following section). Here $\tilde{\chi}_c$ denotes the commanded intercept course based on the helmsman behavior, Eq. (6), displayed in Fig. 3, and constructed as

$$\tilde{\chi}_c = \sigma(y_s) \triangleq \tilde{\chi}_{\text{icpt}} \frac{e^{-(a/2)y_s} - 1}{e^{-(a/2)y_s} + 1} \tag{11}$$

where a and $\tilde{\chi}_{\text{icpt}}$ are positive design parameters. This form for $\sigma(y_s)$ satisfies the conditions (5) and is referred to as a "sigmoidal" function or "squashing" function in the neural network literature. An alternative is the $\arctan(\cdot)$ function. The derivative signal $\dot{\chi}_c$ is constructed as

$$\dot{\chi}_c = \frac{\mathrm{d}}{\mathrm{d}t}\sigma(y_s) = \sigma_{y_s}\frac{\mathrm{d}y_s}{\mathrm{d}t} = \sigma_{y_s} V_g \sin(\tilde{\chi})$$

where

$$\sigma_{y_s} \triangleq \frac{\mathrm{d}}{\mathrm{d}y_s}\sigma(y_s) = -a\,\tilde{\chi}_{\text{icpt}} \frac{e^{-(a/2)y_s}}{\left(e^{-(a/2)y_s} + 1\right)^2}$$

Notice that the slope of $\sigma(y_s)$ at $y_s = 0$ equals $-a\tilde{\chi}_{\text{icpt}}$.

In a coordinated turn, the bank angle is kinematically related to the turn rate as

$$\tan(\phi) = (V_g/g)\dot{\chi} \tag{12}$$

Therefore, commanded course rate of change is mapped to commanded bank angle as

$$\phi_c = \arctan[(V_g/g)\nu] \tag{13}$$

where ν is a pseudocontrol signal designed to provide desired closed-loop behavior,

$$\dot{\chi} = \nu \tag{14}$$

III. Stability Assessment

The course convergence dynamics expressed in Eq. (8) ignores the aircraft dynamics. Stability properties of the guidance law are affected by inner-loop dynamics, specifically those affecting bank angle and yaw rate.

The UAV (an Aerosonde aircraft[22]) is capable of coordinated turns, including turns under moderate turbulence conditions and aggressive maneuvering. With the assumption of coordinated turns, a linear analysis of the Aerosonde operating at constant V_g reveals a behavior between bank-angle command and course rate of change that may be approximated as (with some abuse of notation)

$$\dot{\chi}/\phi_c = b_r/(s + a_r) \tag{15}$$

where s is the Laplace variable, and a_r and b_r are two positive constants based on the roll response and ground speed, respectively $a_r \approx 3.0$ and $b_r \approx 1.2$. (In fact, about zero bank angle $a_r = 1/\tau_\phi$, $b_r = g/V_g/\tau_\phi$, and the ratio $a_r/b_r = V_g/g$, where τ_ϕ is the time constant associated with the aircraft bank angle response $\dot{\phi} = -1/\tau_\phi\phi + 1/\tau_\phi\phi_c$.)

To simplify notation, we temporarily consider the desired path as a constant course north; that is, $\chi_s \equiv 0$, and therefore drop the tilde notation. The effect of curvature is considered subsequently. A bank angle command may be constructed using Eq. (13), and

$$\nu = -k_d\dot{\chi} + k_{d0}(\dot{\chi}_c - \dot{\chi}) + k_p(\chi_c - \chi) + \nu_k \tag{16}$$

of which Eq. (10) is one specific version. The variables k_d, k_{d0}, k_p can be selected to place the poles and zero of the closed-loop Eqs. (13), (15), and (16). For simplicity of the following analysis, select $\nu_k = 0$ and $k_{d0} = 0$. In the neighborhood of the origin $\{\dot{\chi}, \Delta\chi\}$, Eqs. (13) and (16) imply that

$$\phi_c = -(V_g/g)k_d\dot{\chi} + (V_g/g)k_p(\chi_c - \chi) \tag{17}$$

The closed loop becomes

$$\ddot{\chi} + [a_r + b_r(V_g/g)k_d]\dot{\chi} + b_r(V_g/g)k_p\chi = b_r(V_g/g)k_p\chi_c \tag{18}$$

If consistent behavior independent of ground speed is desired, the gains should be designed for a desired frequency and damping ration, $\{\zeta, \omega_n\}$, as

$$k_d = (g/V_g)[(2\zeta\omega_n - a_r)/b_r] \tag{19}$$

$$k_p = (g/V_g)\left(\omega_n^2/b_r\right) \tag{20}$$

With this, the vehicle is able to track a course command with its closed loop behavior governed by

$$\ddot{\chi} + 2\zeta\omega_n\dot{\chi} + \omega_n^2\chi = \omega_n^2\chi_c \tag{21}$$

To use this closed-loop behavior to guide a vehicle along a desired path, the control signal χ_c may be constructed as a function of "cross-track error" y_s. This function reflects a particular helmsman logic. A common logic is a pursuit-guidance law, for example,

$$\chi_c(y_s) = -\arctan(y_s/d) \tag{22}$$

where d is a constant "look-ahead" or "preview" distance. The helmsman logic used in the current work, expressed for a straight course north, is

$$\chi_c = \sigma(y_s) \tag{23}$$

where the sigmoidal function is defined in Eq. (11). Define $k_p' \triangleq b_rV_g/g_ok_p$ and $k_d' \triangleq b_rV_g/g_ok_d$. Combination of kinematics and this design results in the following dynamics:

$$\ddot{\chi} = -(a_r + k_d')\dot{\chi} - k_p'\chi + k_p'\sigma(y_s) \tag{24}$$

$$\dot{y}_s = V_g\sin\chi \tag{25}$$

With $\sigma(y_s) = -a\tilde{\chi}_{\text{icpt}}y_s + \mathcal{O}(y_s^3)$, and ignoring the effect of χ on V_g, we get the behavior about the unique equilibrium, $\{r, \chi, y_s\} = \{0, 0, 0\}$, characterized by the eigenvalues of the matrix

$$\begin{pmatrix} -(a_r + k_d') & -k_p' & -k_p'a\tilde{\chi}_{\text{icpt}} \\ 1 & 0 & 0 \\ 0 & V_g & 0 \end{pmatrix} \tag{26}$$

Its characteristic equation is

$$s^3 + (a_r + k_d')s^2 + k_p's + k_p'a\tilde{\chi}_{\text{icpt}}V_g = 0 \tag{27}$$

For stability, the Routh–Hurwitz criterion results in the following condition:

$$k_p' - V_g\frac{k_p'a\tilde{\chi}_{\text{icpt}}}{(a_r + k_d')} > 0 \tag{28}$$

This reveals that, to avoid unstable coupling of aircraft dynamics and helmsman guidance, the helmsman sensitivity represented by the product $a\tilde{\chi}_{\text{icpt}}$ should be limited by

$$a\tilde{\chi}_{\text{icpt}} < (a_r + k_d')/V_g \tag{29}$$

For a closed loop bank angle dynamics design with $\{\zeta, \omega_n\}$ as suggested earlier, this result implies that

$$a\tilde{\chi}_{\text{icpt}} < 2\zeta\omega_n/V_g \tag{30}$$

that is, the intercept angle can be larger for more aggressive bank-angle dynamics, and is inversely proportional to the ground speed.

This analysis holds for the tracking of a straight line. Nonzero curvature and use of a lookahead or preview distance also affect this result. In implementation, the actual values for a and $\tilde{\chi}_{\text{icpt}}$ satisfied this criterion even with aggressive intercept angles. However, to ensure stability, it may be necessary to schedule the intercept angle with ground speed.

If the control law Eq. (16) is used for following a curved path, the absence of integral action will lead to steady state error. The effect of curvature can be accounted for with Serret–Frenet kinematics, assuming that V_g does not change rapidly. When the aircraft is on the path with constant curvature κ, and inertial speed V_g, the steady state rate of turn is $\dot{\chi} = \kappa V_g$. (Strictly speaking this is not steady state because $V_g(t)$ is continuously changing if constant airspeed is maintained. However, these changes occur at a slower time scale than the bank angle dynamics.)

We may rewrite Eqs. (24) and (25) for the curved path situation,

$$\ddot{\chi} = -a_r(\dot{\chi} - \kappa V_g) + b_r(\phi_c - \phi_\kappa) \tag{31}$$

$$\dot{\tilde{\chi}} = (\dot{\chi} - \kappa V_g) - \kappa^2 V_g y_s \tag{32}$$

$$\dot{y}_s = V_g\tilde{\chi} \tag{33}$$

where ϕ_κ is the trim bank angle, and the notion of being on the path is included in the sense that

$$\dot{s} = V_g[\cos\tilde{\chi}/(1 - \kappa y_s)] \approx V_g(1 + \kappa y_s) \tag{34}$$

and therefore $\dot{s} - V_g \approx V_g\kappa y_s$, which leads to Eq. (32) because

$$\dot{\tilde{\chi}} = \dot{\chi} - \dot{\chi}_s = \dot{\chi} - \kappa\dot{s} = (\dot{\chi} - \kappa V_g) - \kappa(\dot{s} - V_g)$$

The trim bank angle from Eq. (31) can be seen to be approximately

$$\phi_\kappa = (a_r/b_r)\kappa V_g \tag{35}$$

In fact, the trim bank angle reflects a steady state response, which is a kinematic expression of a truly banked or coordinated turn independent of vehicle characteristics:

$$\phi_\kappa = \arctan\left[(V_g/g)\dot{\chi}\right] = \arctan\left[\kappa\left(V_g^2/g\right)\right] \tag{36}$$

Therefore, we can design the kinematic feedforward term in the control law, Eq. (10), as the product of curvature and inertial speed,

$$\nu_\kappa = \kappa V_g \tag{37}$$

About the trim bank angle, the effect of the control law Eq. (10) is approximately

$$\phi_c \approx \bar{k}_p(\tilde{\chi}_c - \tilde{\chi}) + \phi_\kappa \tag{38}$$

and therefore

$$\phi_c - \phi_\kappa \approx -\bar{k}_pa\tilde{\chi}_{\text{icpt}}y_s - \bar{k}_p\tilde{\chi} \tag{39}$$

where

$$\bar{k}_p \triangleq V_g/g\left\{1+(\nu_\kappa V_g/g)^2\right\}^{-1} \tag{40}$$

Thus, the dynamics of Eqs. (31–33) can be approximated about the equilibrium $\{\dot{\chi}-\kappa V_g, \tilde{\chi}, y_s\}=\{0,0,0\}$ as

$$\frac{\mathrm{d}}{\mathrm{d}t}(\dot{\chi}-\kappa V_g, \tilde{\chi}, y_s)^T = M(\dot{\chi}-\kappa V_g, \tilde{\chi}, y_s)^T \tag{41}$$

where

$$M=\begin{pmatrix} -a_r & -b_r\bar{k}_p & -b_r\bar{k}_p a\tilde{\chi}_{\text{icpt}} \\ 1 & 0 & -V_g\kappa^2 \\ 0 & V_g & 0 \end{pmatrix} \tag{42}$$

Applying the Routh–Hurwitz criterion as before, the limiting gain for the helmsman can be shown to be as in Eq. (29) (with $k_d=0$) and thus it can be shown that the curvature does not cause instability. (However, it can be shown that curvature affects damping.) Reference 10 shows that when a pursuit–guidance type helmsman as in Eq. (22) is used, the gain limit for straight-path convergence is a conservative estimate for convergence to a curved path.

IV. Gimbal Kinematics and Path Geometry

A. Problem Description

We are interested in maneuvers that allow maximum exposure of a target in the face of aircraft and camera limitations. We refer to the results as "maneuvers" because they are not necessarily trimmed-flight solutions. Rather, the resulting state trajectories are defined by observation geometry and the fact that the aircraft maintains coordinated flight. The commanded bank angle is limited to ±30 deg for mild maneuvering and ±45 deg for more aggressive maneuvers. The roll rate is limited to ±45 deg/s.

The aim of the path design is to manipulate the position of the target relative to the aircraft. Therefore, it is advantageous to approach the maneuver from a pilot's perspective and find corresponding field-of-view patterns. Thomasson[1] found analytic expressions for flight that result in a constant line-of-sight tilt angle based on assumptions such as level flight, no wind, and small α. In this work, we follow a similar development, and find analytical expressions for camera angles and zoom as function of yaw, yaw rate, altitude, velocity, and wind velocity, including the possibility of using a nonzero sideslip angle.[2] The objectives in studying these maneuvers are

1) Analytical expressions for path parameters, as functions of clock angle.

2) A feedback mechanism of path parameters to construct guidance signals.

3) Target exposure assessment and required camera turret activity.

4) Minimization of heuristics in implementation.

To establish the problem of limited target exposure, we first look at a circle in wind, on "turn-about-a-point," that is, given the maneuver we find the corresponding geometry. Next, we address the more interesting problem of the wind ellipse, or "turn-on-a-pylon,"[26] where the observation geometry defines the maneuver. In the wind ellipse, the wingtip points at the target throughout the maneuver, while the aircraft maintains coordinated flight.

B. Camera Gimbal Kinematics

The camera angles needed to keep the target in sight are based on aircraft pose (position and orientation) and target location. Figure 4 presents the geometry for tilt, pan, and zoom. The gimbal angles can be determined using analytic expressions based on the four-quadrant inverse tangent function and using the relative position and aircraft attitude information. The steps are as follows:

1) Obtain a normalized line of sight (LOS) for the relative position of aircraft and target:

$$\widehat{\text{los}}|_e = \frac{[x_{\text{tgt}}, y_{\text{tgt}}, z_{\text{tgt}}]_e^T - [x_{\text{ac}}, y_{\text{ac}}, z_{\text{ac}}]_e^T}{\left\|[x_{\text{tgt}}, y_{\text{tgt}}, z_{\text{tgt}}]_e^T - [x_{\text{ac}}, y_{\text{ac}}, z_{\text{ac}}]_e^T\right\|}$$

2) Find the normalized line-of-sight, vector expressed in the aircraft body frame,

$$[\hat{x}_{\text{los}}, \hat{y}_{\text{los}}, \hat{z}_{\text{los}}]_b^T = {}_bT_e(\phi,\theta,\psi)\widehat{\text{los}}|_e$$

3) Obtain camera angle κ using the LOS components in the body frame as (arctan is implemented as the four quadrant inverse tangent)

$$\kappa = \arctan(\hat{z}_{\text{los}}, \hat{x}_{\text{los}})$$

4) Find λ using the LOS components in the body frame as

$$\lambda = \arctan\left(\hat{y}_{\text{los}}, \sqrt{\hat{x}_{\text{los}}^2+\hat{z}_{\text{los}}^2}\right)$$

C. Camera Gimbal Limit Problem Demonstration

Figures 5 and 6 indicate the effect of gimbal angle saturation in a circular orbit with wind. These figures display traces of simulated flight of an Aerosonde aircraft[22,23] with a nose-mounted gimbaled camera flying in moderate turbulence. The camera pan angle saturates at time $t \approx 75$ s and onwards. To reduce the target-out-of-sight

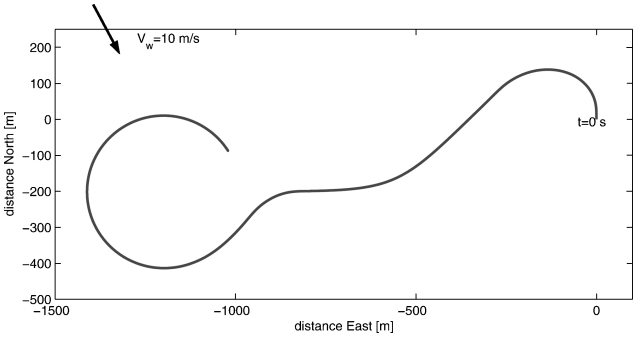

Fig. 5 Flight trajectory of 1.5 min, with initial aircraft heading north, $V_w = 10$ m/s, and $V_a \approx 25$ m/s.

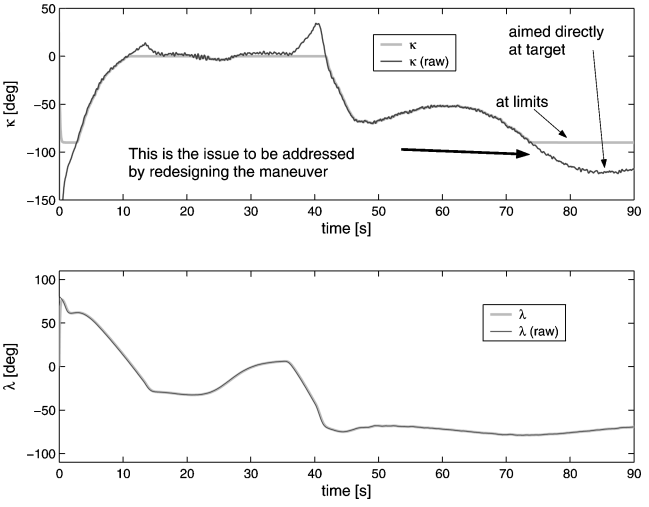

Fig. 6 Corresponding gimbal angles. The bank-angle requirements are reflected in the requirements on the tilt angle necessary for target capture. However, the most stringent requirements are placed on the pan-angle capabilities. The last 20 s of the κ time history displays that the wind-correction requires a κ beyond the pan range. The effects of turbulence are also more pronounced in the κ channel (associated with pitch motion) than in the λ channel (roll).

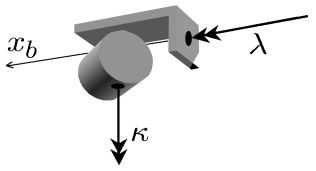

Fig. 4 Geometry for nose-mounted camera: pan angle κ and tilt angle λ.

problem, we wish to find the trajectory that maintains the geometry between vehicle and target constant. Two possible scenarios are considered, both assuming coordinated flight:

1) Maintaining constant pan angle, equivalent to maintaining a constant angle between x_b axis and line-of-sight (e.g., keep target at two-o'-clock).

2) Maintaining both pan and tilt angle constant. This will require changes in altitude and/or airspeed.

For target observation these maneuvers have the advantage of increased camera stability due to the larger inertia about the x_b axis and the natural aerodynamic damping in roll. An example of the second maneuver is orienting the wingtip at the target throughout the orbit. However, for most small UAVs the pivotal altitude will likely be too low to be practicable.

D. Path Geometry for Constant Line of Sight

Using reasoning similar to that for Ref. 1, but explicitly allowing for wind from arbitrary direction χ_w, with angular position of the vehicle determined by bearing from the target or clock angle ψ_p, and the relative position of the target measured from the x_b-axis clockwise ζ. Hence, ζ is from the pilot's perspective; $\zeta = 60$ deg corresponds to a pilot having the target at his/her two-o'-clock position. The expression for the change in radius as a function of the relative position is

$$\frac{\mathrm{d}r}{\mathrm{d}\psi_p} = r\frac{-V_a c_\zeta - V_w c_{\psi-\chi_w+\zeta}}{V_a s_\zeta + V_w s_{\psi-\chi_w+\zeta}} \tag{43}$$

which can be expressed in terms of ψ_p by the relation

$$\psi_p = \zeta + \psi - \pi \tag{44}$$

The trigonometric relations

$$c_{\psi-\chi_w+\zeta} = -c_{\psi_p}c_{\chi_w} - s_{\psi_p}s_{\chi_w}$$

$$s_{\psi-\chi_w+\zeta} = c_{\psi_p}s_{\chi_w} - s_{\psi_p}c_{\chi_w}$$

allow the expression

$$\frac{\mathrm{d}r}{\mathrm{d}\psi_p} = r\frac{-V_a c_\zeta + V_w\left(c_{\psi_p}c_{\chi_w} + s_{\psi_p}s_{\chi_w}\right)}{V_a s_\zeta + V_w\left(c_{\psi_p}s_{\chi_w} - s_{\psi_p}c_{\chi_w}\right)} \tag{45}$$

The special case where the target remains under the wingtip throughout the maneuver, $\zeta = \pi/2$, can be presented as

$$\frac{\mathrm{d}r}{\mathrm{d}\psi_p} = r\frac{V_w\left(c_{\psi_p}c_{\chi_w} + s_{\psi_p}s_{\chi_w}\right)}{V_a - V_w\left(s_{\psi_p}c_{\chi_w} - c_{\psi_p}s_{\chi_w}\right)} \tag{46}$$

The radius of the orbit can be found by integration of Eq. (45). For $\zeta < \pi/2$ this requires numerical integration; for the special case $\zeta = \pi/2$ the result is

$$r(\psi_p) = r_0\frac{V_a + V_w s_{\chi_w}}{V_a - V_w s_{\psi_p-\chi_w}} \tag{47}$$

where $r_0 = r(\psi_p = 0)$ is the radius directly north of the target, Fig. 7. Equation (47) represents an elliptical orbit that maintains the wingtip in the direction of, though not necessarily pointed directly at, the target. Hence, it results in a constant camera pan angle κ, with tilt angle depending on the vehicle bank angle. To maintain a relative angle $\zeta < \pi/2$ requires a spiral trajectory toward the target.[1]

The minimum radius in the elliptical orbit is related to r_0 by

$$r_{\min} = r_0\frac{V_a + V_w}{V_a + V_w s_{\chi_w}}$$

In terms of the minimum radius, the path can be expressed as

$$r(\psi_P) = r_{\min}\frac{V_a + V_w}{V_a - V_w s_{\psi_P-\chi_w}} \tag{48}$$

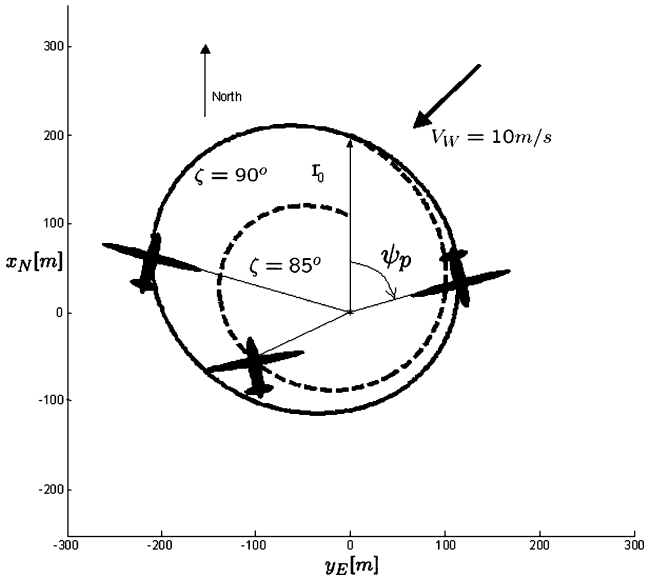

Fig. 7 Elliptical orbit for $\zeta = 90$ deg, Eq. (47), and spiral trajectory in wind from numeric integration of Eq. (45) with $\zeta = 85$ deg. Target at origin. $V_a = 25$ m/s, $V_w = 10$ m/s from 45 deg.

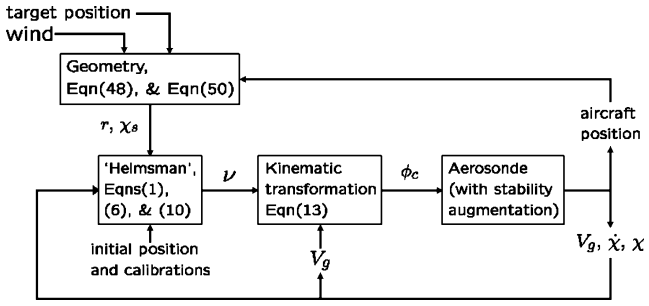

Fig. 8 The structure of the simulation demonstration. The Aerosonde aircraft dynamics and environmental model were obtained from Ref. 23.

where the minimum radius occurs at $\psi_P = \chi_w + \pi/2$ when the UAV is flying clockwise about the target. The ground speed is of a maximum at this point, $V_g = V_a + V_w$. Hence, given a maximum bank angle, $\phi_{\max}$, the minimum possible radius is

$$r_{\min} = \frac{(V_a + V_w)^2}{g t_{\phi\max}} \tag{49}$$

The desired course for the elliptical spiral trajectory is

$$\chi_s(\psi_P) = \arctan\left(\frac{V_w c_{\chi_w} + V_a c_{\psi_P-\zeta}}{-V_a s_{\psi_P-\zeta} - V_w s_{\chi_w}}\right)$$

From this expression, the desired course for wingtip at target, that is, $\zeta = \pi/2$, is constructed as

$$\chi_s(\psi_P) = \arctan\left(\frac{V_w c_{\chi_w} - V_a s_{\psi_P}}{-V_a c_{\psi_P} - V_w s_{\chi_w}}\right) \tag{50}$$

V. Demonstration of Results

The effectiveness of these results can be demonstrated in a simulation environment. Figure 8 displays the structure of the simulation, which represents the integration of the orbit formulated in terms of the desired course, the propagation of the Serret–Frenet formulation, the helmsman, and the Aerosonde aircraft. The aircraft is exposed to atmospheric turbulence and windshear modeling, using the default values in the Aerosim Blockset of Ref. 23. Using this dynamics model and assuming a nose-mounted gimballed camera as

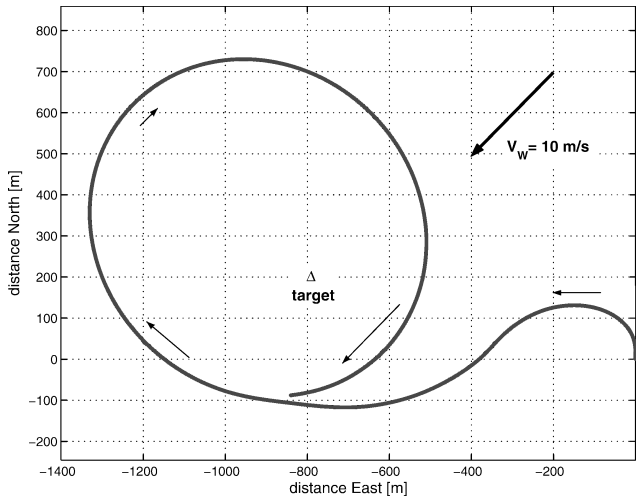

Fig. 9 Approaching the target on a course of 270 deg, with wind 45 deg at 10 m/s. The information used to commence the orbit capture is distance to target, $d \leq 2r_0$, where $r_0 = 500$ m is the distance north of target. The minimum radius is related to r_0 as given by Eq. (49). The path parameters y_s and ψ_s are determined by Eqs. (48) and (50).

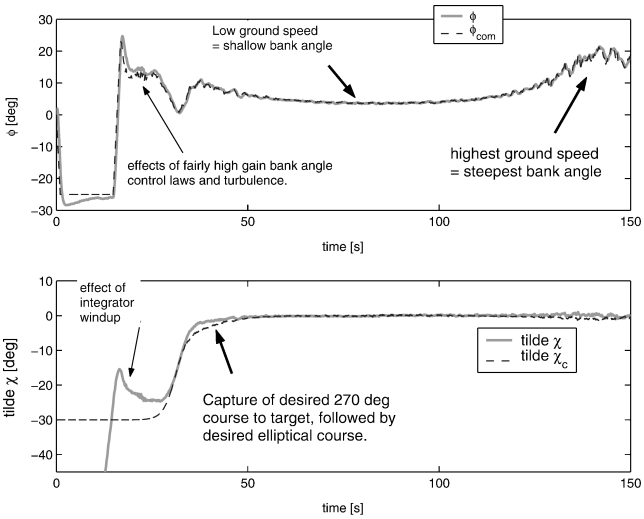

Fig. 10 Bank angle and relative course time histories corresponding to Fig. 9. Noise is due to Dryden moderate turbulence modeling and an aggressive bank-angle control law.

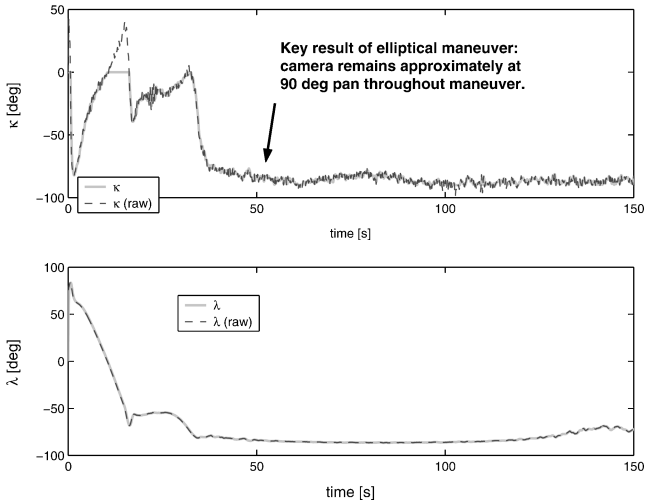

Fig. 11 Camera gimbal angles corresponding to Fig. 9. The key result of this maneuver is that the aircraft orients its wingtip over the target throughout the maneuver.

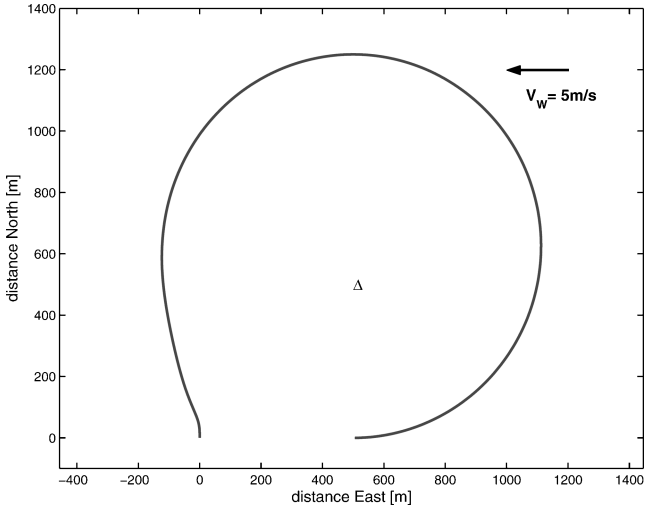

Fig. 12 On-pylon maneuver: trajectory of 150 s of flight orbiting target at approximate pivotal altitude in light wind and turbulence. Target located at {North, East} = {500, 500} m, wind 90 deg at 5 m/s.

described in Sec. IV.B, Figs. 9–11 display the results, which should be compared with those in Figs. 5 and 6.

If in addition we allow the altitude to change, we can operate the aircraft at pivotal altitude[25] to maintain the wingtip pointed at the target. Expressions (48–50) define the path geometry for constant line-of-sight observation. When flown at pivotal altitude, this results in the target being fixed at the wingtip from the perspective of the $\mathcal{F}_b$ frame. These expressions can all be updated as wind-speed and direction estimates become available. To demonstrate this, the aircraft is augmented with a simple altitude tracker based on proportional feed back of altitude error to the engine power setting. The feedback is filtered with a settling time of 1 s. Airspeed is maintained by means of pitch. The results are displayed in Figs. 12–16. The drawback of a path at pivotal altitude is that the relatively low speeds of the UAV will require an altitude that will likely be too low for safety and robustness considerations, and depending on the ratio V_g/V_w, the required altitude changes can be excessive.

VI. Wind Estimate

The path-following algorithm is robust with respect to wind and does not rely on knowledge of wind and heading. However, the constant line-of-sight geometry requires local wind information. The camera field of view is robust enough to allow approximate solutions, relying on estimates of wind speed and direction. An error in wind estimate would result in the target wandering in the camera field of view. This section describes a means to continuously estimate the wind speed and direction.

The airspeed V_a is measured with air data instruments, the ground speed V_g and course χ are measured by GPS, and wind speed V_w and direction χ_w are related to the aircraft heading, ψ, for example, in north and east directions as

$$V_g c_\chi = V_a c_\psi - V_w c_{\chi_w} \triangleq V_a c_\psi + u_w$$

$$V_g s_\chi = V_a s_\psi - V_w s_{\chi_w} \triangleq V_a s_\psi + v_w$$

If wind speed and direction are considered constant (slowly varying), then these can be considered as unknown initial conditions and obtained by means of an observer. Assuming that the aircraft heading is measured, a nonlinear observer may be constructed to estimate the wind direction and speed. An approach similar to that of Ref. 27 is used:

$$\frac{\mathrm{d}}{\mathrm{d}t}\hat{\boldsymbol{x}} = A_o\hat{\boldsymbol{x}} + B_o\boldsymbol{u}_o \tag{51}$$

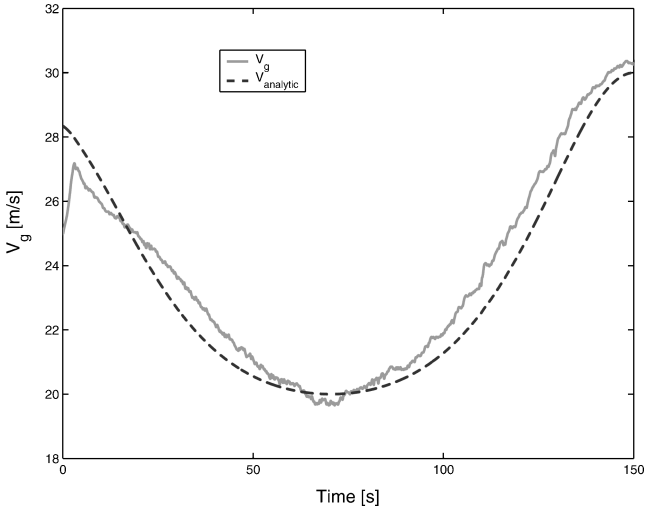

Fig. 13 Inertial speed corresponding to Fig. 12. $V_a \approx 25$ m/s in turbulence.

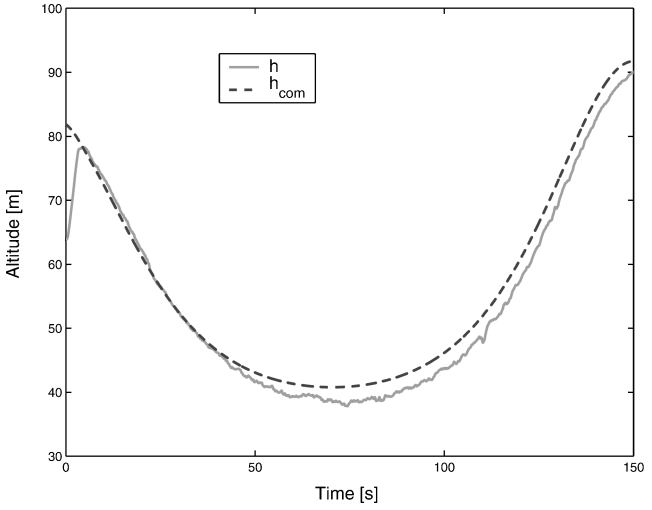

Fig. 14 Pivotal altitude and actual altitude time histories corresponding to Fig. 12. Altitude (flight path) is controlled with throttle.

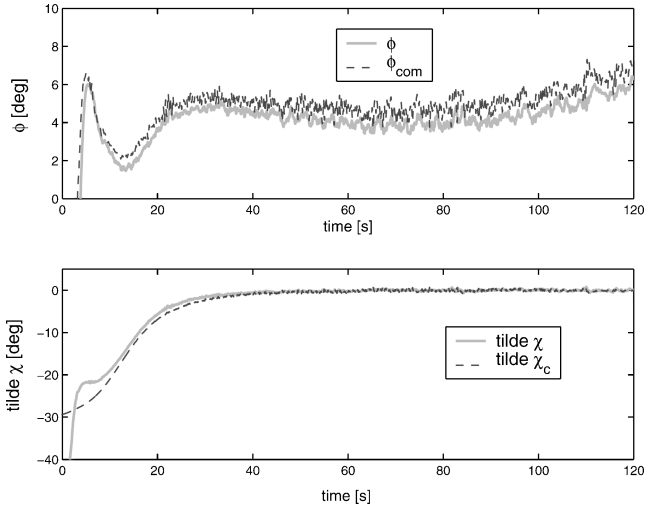

Fig. 15 Bank angle and relative course time histories corresponding to the first 2 min of Fig. 12. Aircraft converges with exact ellipse at about $t = 30$ s.

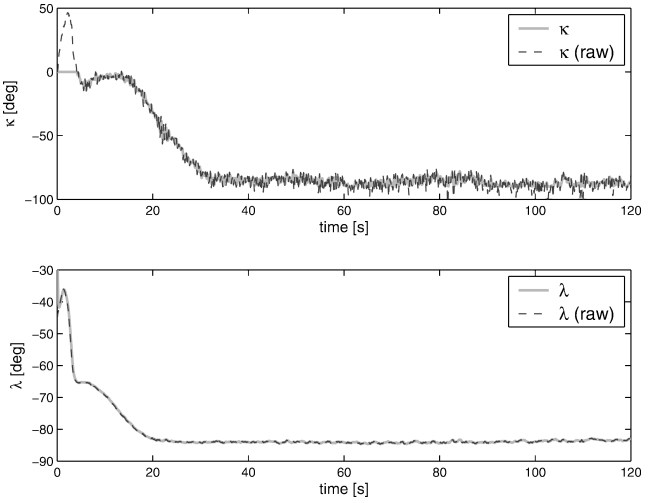

Fig. 16 Keeping the camera aiming efforts to a minimum: gimbal angles corresponding to first 2 min of Fig. 12. The purpose of this maneuver is to maintain tilt-angle λ near constant, while κ is also maintained near constant.

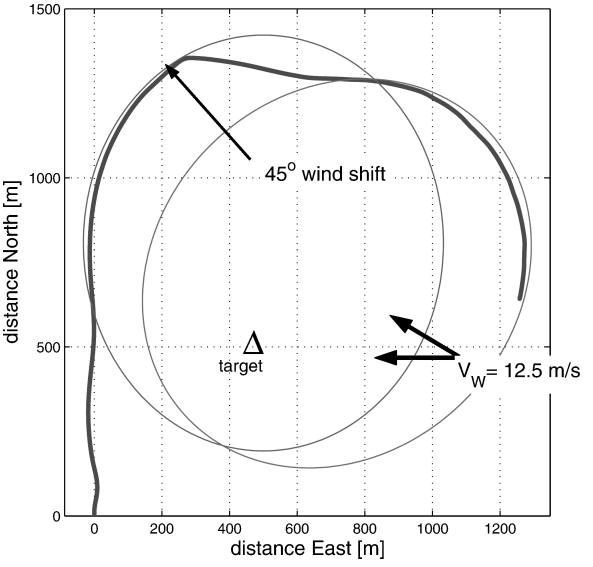

Fig. 17 Integration of wind estimator with observation orbit orientation. Displayed is the path of a 3-min flight at an airspeed of $V_a = 25$ m/s, with wind 90 deg at 12.5 m/s. The initial target path is an ellipse with a minimum radius of 300 m. North-northeast of the target, the aircraft is exposed to a southerly windshift of 45 deg occurring over 10 s. The new wind direction and speed is observed and subsequently used to reorient the desired path for constant observation angle.

where

$$\hat{\boldsymbol{x}}^T = (\hat{x}, \hat{y}, \hat{u}_w, \hat{v}_w), \qquad \boldsymbol{u}_o^T = (x_N, y_E, V_a c_\psi, V_a s_\psi)$$

and

$$A_o = \begin{pmatrix} -\lambda_1 & 0 & 1 & 0 \\ 0 & -\lambda_2 & 0 & 1 \\ -\lambda_3 & 0 & 0 & 0 \\ 0 & -\lambda_4 & 0 & 0 \end{pmatrix}, \qquad B_o = \begin{pmatrix} \lambda_1 & 0 & 1 & 0 \\ 0 & \lambda_2 & 0 & 1 \\ \lambda_3 & 0 & 0 & 0 \\ 0 & \lambda_4 & 0 & 0 \end{pmatrix}$$

This results in a linear error model as

$$\dot{\tilde{x}} = -\lambda_1 \tilde{x} + \tilde{u}_w, \qquad \dot{\tilde{y}} = -\lambda_2 \tilde{y} + \tilde{v}_w$$

$$\dot{\tilde{u}}_w = -\lambda_3 \tilde{x}, \qquad \dot{\tilde{v}}_w = -\lambda_4 \tilde{y}$$

where $\tilde{x} \triangleq x - \hat{x}$, et-c. A demonstration is displayed in Fig. 17.

VII. Conclusions

A path-following algorithm has been described and demonstrated for autonomous observation of a target from a UAV with a nose-mounted camera.

Small UAVs will be exposed to wind speeds that are a significant portion of the UAV flight speed. This affects the ability of the vehicle to aim and stabilize its sensors at a target. In this work, geometric expressions are derived for orbits that allow the aircraft to keep its wingtip aimed at the target, that is, flight paths that result in constant line of sight with respect to the aircraft body-fixed frame.

It is shown that camera angles can be maintained near constant. Furthermore, the image quality benefits from the natural roll damping of the aircraft which reduces the effects of turbulence. Use of these orbits greatly reduce the potential for operator disorientation, and allow a reference for remote camera operation.

An observer for wind speed and direction is also demonstrated, which continuously estimates the proper orientation of the orbits about the targets. Wind estimation errors do not significantly affect the target imaging.

Acknowledgments

This work was supported by the University of Washington, Royalty Research Fund Grant 65-1914, The Insitu Group, and Hood Technology Corporation. Marius Niculescu provided the Aerosonde dynamics and environmental model.

References

[1]Thomasson, P. G., "Guidance of a Roll-Only Camera for Ground Observation in Wind," *Journal of Guidance, Control, and Dynamics*, Vol. 21, No. 1, 1998, pp. 39–44.

[2]Stolle, S., and Rysdyk, R., "Flight Path Following Guidance for Unmanned Air Vehicles with Pan-Tilt Camera for Target Observation," *Proceedings of the IEEE Digital Avionics Systems Conference*, Vol. 2, IEEE Publications, Piscataway, NJ, Oct. 2003, pp. 8B3, 1–12.

[3]Lee, J., Huang, R., Vaughn, A., Xiao, X., and Hedrick, J. K., "Strategies of Path-Planning for a UAV to Track a Ground Vehicle," *Proceedings of the 2nd Annual Autonomous Intelligent Networks and Systems Conference*, IEEE Control Systems Society, IEEE Publications, Piscataway, NJ, 2003.

[4]Frew, E. W., Xiao, X., Spry, S., McGee, T., Kim, Z., Tisdale, J., Sengupta, R., and Hedrick, J. K., "Flight Demonstrations of Self-Directed Collaborative Navigation of Small Unmanned Aircraft," AIAA Paper 2004-6608, Sept. 2004.

[5]Frezza, R., and Altafini, C., "Autonomous Landing by Computer Vision: An Application of Path Following in SE(3)," *Proceedings of the 39th IEEE Conference on Decision and Control*, IEEE Publications, Piscataway, NJ, Dec. 2000, pp. 2527–2532.

[6]Frezza, R., "Path Following for Air Vehicles in Coordinated Flight," *Proceedings of the 1999 IEEE/ASME International Conference on Advanced Intelligent Mechatronics*, pp. 884–889.

[7]Rysdyk, R., Lum, C. W., and Vagners, J., "Autonomous Orbit Coordination for Two Unmanned Aerial Vehicles," AIAA Paper 2005-6362, Aug. 2005.

[8]"Unmanned Aerial Vehicles Roadmap 2002–2027," Dept. of Defense Memorandum, Washington, DC, Dec. 2002.

[9]Papoulias, F. A., "Bifurcation Analysis of Line-of-Sight Vehicle Guidance Using Sliding Modes," *International Journal of Bifurcation and Chaos*, Vol. 1, No. 4, 1991, pp. 849–865.

[10]Papoulias, F. A., "On the Nonlinear Dynamics of Pursuit Guidance for Marine Vehicles," *Journal of Ship Research*, Vol. 37, No. 4, 1993, pp. 342–353.

[11]Papoulias, F. A., "Cross Track Error and Proportional Turning Rate Guidance of Marine Vehicles," *Journal of Ship Research*, Vol. 38, No. 2, 1994, pp. 123–132.

[12]Kaminer, I., Pascoal, A., Hallberg, E., and Silvestre, C., "Trajectory Traking for Autonomous Vehicles: An Integrated Approach to Guidance and Control," *Journal of Guidance, Control, and Dynamics*, Vol. 21, No. 1, 1998, pp. 29–38.

[13]Hauser, J., and Hindman, R., "Manuever Regulation from Trajectory Tracking: Feedback Linearizable Systems," *Proceedings of the International Federation of Automatic Control, Nonlinear Control System Design*, 1995, pp. 595–600.

[14]Hauser, J., and Hindman, R., "Manuever Regulation from Trajectory Tracking: Feedback Linearizable Systems," *Proceedings of the International Federation of Automatic Control, Nonlinear Control System Design*, Pergamon Press, 1995, pp. 595–600.

[15]Skjetne, R., Fossen, T., and Kokotović, P., "Output Maneuvering for a Class of Nonlinear Systems," *Proceedings, 15th International Federation of Automatic Control*, International Federation of Automatic Control, Laxenburg, Austria, July 2002.

[16]Breivik, M., "Nonlinear Maneuvering Control of Underactuated Ships," M.Sc. Thesis Rept., Norwegian University of Science and Technology, June 2003.

[17]Fossen, T., Breivik, M., and Skjetne, R., "Line-of-Sight Path Following of Underactuated Marine Craft," *Proceedings, 6th International Federation of Automatic Control on Marine Craft Maneuvering and Control*, 2003.

[18]Park, S., Deyst, J., and How, J., "A New Nonlinear Guidance Logic for Trajectory Tracking," AIAA Paper 2004-4900, Aug. 2004.

[19]Aicardi, M., Casaline, G., Indiveri, G., Aguiar, A., Encarnacao, P., and Pascoal, A., "A Planar Path Following Controller for Underactuated Marine Vehicles," *9th IEEE Mediterranean Conference on Control and Automation*, Dubrovnik, June 2001.

[20]Skjetne, R., and Fossen, T., "Nonlinear Maneuvering and Control of Ships," *Proceedings of the IEEE Marine Technology Society & Oceanic Engineering Society Conference 2001*, IEEE Publications, Piscataway, NJ, Nov. 2001, pp. 1808–1815.

[21]Pettersen, K., and Lefeber, E., "Way-Point Tracking Control of Ships," *Proceedings 40th IEEE Conference on Decision and Control*, IEEE Publications, Piscataway, NJ, Dec. 2001, pp. 940–945.

[22]The Insitu Group Inc., "Aerosonde" [Web site], URL: http://www.insitugroup.net/Pages/aerosonde.html [cited 10 Nov. 2005].

[23]Unmanned Dynamics LLC., "Dynamic Model of Aerosonde UAV" [Web site], URL: http://www.u-dynamics.com/aerosim/ [cited 10 Nov. 2005].

[24]Rathbun, D., Kragelund, S., Pongpunwattana, A., and Capozzi, B., "An Evolution Based Path Planning Algorithm for Autonomous Motion of a UAV Through Uncertain Environments," *Proceedings of the IEEE Digital Avionics Systems Conference*, Vol. 2, 2002, pp. 8D2, 1–12.

[25]Johnson, E. N., "Limited Authority Adaptive Flight Control," Ph.D. Dissertation, Georgia Inst. of Technology, Atlanta, Dec. 2000.

[26]Denker, J. S., *See How It Flies* [on-line book], Section 16.16: Eights and Turns on Pylons, URL: http://www.av8n.com/how/htm/maneuver.html [cited 10 Nov. 2005].

[27]Encarnaçao, Pascoal, and Arcak, "Path Following for Autonomous Marine Craft," *Proceedings of the 5th International Federation of Automatic Control Conference on Marine Craft Maneuvering and Control*, Aug. 2000, pp. 117–122.